RSC Advances

Three-dimensional polymer scaffolds with interconnected porous structures were fabricated by thermally induced phase separation of novel biodegradable poly(propylene fumarate)-*co*-poly(L-lactic acid).

RSC Advances

PAPER

Novel biodegradable poly(propylene fumarate)-*co*-poly(L-lactic acid) porous scaffolds fabricated by phase separation for tissue engineering applications

Xifeng Liu,[ab] A. Lee Miller II,[ab] Brian E. Waletzki,[ab] Michael J. Yaszemski,[ab] and Lichun Lu[*ab]

Scaffolds with intrinsically interconnected porous structures are highly desirable in tissue engineering and regenerative medicine. In this study, three-dimensional polymer scaffolds with highly interconnected porous structures were fabricated by thermally induced phase separation of novel synthesized biodegradable poly(propylene fumarate)-*co*-poly(L-lactic acid) in a dioxane/water binary system. Defined porous scaffolds were achieved by optimizing conditions to attain interconnected porous structures. The effect of phase separation parameters on scaffold morphology were investigated, including polymer concentration (1, 3, 5, 7, and 9%), quench time (1, 4, and 8 min), dioxane/water ratio (83/17, 85/15, and 87/13 wt/wt), and freeze temperature (−20, −80, and −196 °C). Interesting pore morphologies were created by adjusting these processing parameters, e.g., flower-shaped (5%; 85/15; 1 min; −80 °C), spherulite-like (5%; 85/15; 8 min; −80 °C), and bead-like (5%; 87/13; 1 min; −80 °C) morphology, Modulation of phase separation conditions also resulted in remarkable differences in scaffold porosities (81% to 91%) and thermal properties. Furthermore, scaffolds with varied mechanic strengths, degradation rates, and protein adsorption capabilities could be fabricated using the phase separation method. In summary, this work provides an effective route to generate multi-dimensional porous scaffolds that can be applied to a variety of hydrophobic polymers and copolymers. The generated scaffolds could potentially be useful for various tissue engineering applications including bone tissue engineering.

Introduction

Tissue engineering provides a promising strategy for tissue regeneration and organ repair.[1] One important approach in tissue engineering is *in vitro* culture of autologous cells in a biodegradable three-dimensional (3-D) supporting matrix followed by *in vivo* implantation to tissues with injuries or defects.[2] Materials acting in this process are highly desired to be biodegradable, biocompatible and have excellent chemical, mechanical, and topographical signal transferring abilities at the surfaces to attract the adhesion and growth of cells.[3] Biodegradable polymeric materials, either natural or synthetic, meet many of the design requirements and have been studied extensively for various tissue engineering applications.[4]

In bone tissue engineering, the clinical needs for bone regeneration have motivated extensive research efforts using a multitude of polymers including polyethylene,[5] poly(ethylene glycol) (PEG),[6] poly(ε-caprolactone) (PCL),[7-8] poly(2-hydroxyethyl methacrylate) (pHEMA),[9] poly(methyl methacrylate) (PMMA),[10] poly(L-lactic acid) (PLLA),[11] poly(propylene fumarate) (PPF),[12,13] PPF-*co*-PCL and other copolymers.[14] PLLA and its copolymers have favorable chemical properties such as biodegradability through hydrolysis, physical properties such as high stiffness, and good efficiency in supporting bone regeneration.[15] Animal studies have demonstrated excellent tissue affinities for PLLA-based stents without exhibiting inflammatory reactions.[16,17] As another essential polymer, PPF as well as its copolymers and blends, were evaluated extensively in bone tissue engineering[18,19] and distinct bone cell behaviors have been found.[20]

In a majority of cases, polymer scaffolds were designed to have three-dimensional open porous structures to minimize diffusion limitations thus facilitating cell adhesion, tissue growth and material biodegradation. Common practices to fabricate 3-D composite scaffold including 3-D printing, particulate leaching, microsphere sintering, electrospinning, and thermally induced phase separation (TIPS).[21-22] Among these techniques, TIPS has been explored for producing interconnected porous structures by reducing polymer/solution system temperature across the upper critical solution temperature (UCST).[23] Mechanism for this TIPS process involves the modulation of thermal energy by quench route to induce a homogeneous polymer solution shifting into a solid-liquid phase system. Scaffolds with intrinsically interconnected morphology are then achieved by extracting the liquid component through lyophilization. TIPS technique is facile and controllable, making it a useful methodology for generating porous scaffold architectures.

In this study, we have developed a novel biodegradable triblock PPF-*co*-PLLA copolymer through ring-opening reactions of PPF and L-lactide monomers. TIPS technique was then applied to fabricate interconnected porous PPF-*co*-PLLA scaffolds using a dioxane/water binary system as solvent. Main factors governing liquid–liquid de-mixing for the polymer/solvent system, including PPF-*co*-PLLA

concentration, quench time, freeze temperature, and dioxane/water ratio, were investigated in this study. Moreover, crystallinities associated with the quenching process, and scaffold mechanical strength, hydrophobicity/hydrophilicity as well as protein adsorption were evaluated. To our knowledge, this work is the first report on the fabrication of interconnected porous PPF-*co*-PLLA scaffolds by the TIPS method.

Experimental

Fumaryl chloride, propylene glycol, L-Lactide (3,6-dimethyl-1,4-dioxane-2,5-dione) and tin(II) 2-ethylhexanoate (stannous octoate, $Sn(Oct)_2$, 95%) were purchased from Sigma Aldrich Co. (Milwaukee, WI). Solvents were purchased from Fisher (Pittsburgh, PA) as reagent grade and used as received. All other chemicals and reagents were purchased from Sigma Aldrich Co. (Milwaukee, WI) and used as-is unless noted otherwise.

Synthesis of PPF-*co*-PLLA triblock copolymer
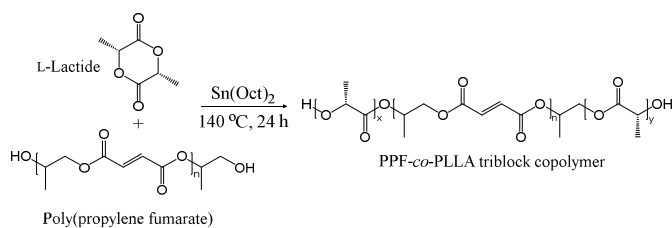
Fig. 1 Schematic view of the synthesis route of PPF-*co*-PLLA triblock copolymer.

Poly(propylene fumarate) was synthesized from diethyl fumarate and 1,2-propylene glycol using hydroquinone as a crosslinking inhibitor and zinc chloride as catalyst, as described previously.[24] Briefly, diethyl fumarate (259 g) and 1,2-propylene glycol (342 g) were mixed together in a three-neck round-bottom flask (2 L), and heated to 100 °C for 1 h, then kept at 150 °C for 7 h to synthesis fumaric diester. In this step, 0.33 g of hydroquinone and 2.04 g of zinc chloride were added as crosslinking inhibitor and catalyst, respectively. The byproduct ethanol and propylene glycol were removed by distillation under nitrogen. Obtained fumaric diester was polycondensed to form linear PPF with hydroxyl groups on both ends. Dried PPF were then copolymerized with L-lactide monomer by a ring opening reaction at 140 °C for 24 hours, as schematically described in Fig. 1. Stannous octoate ($Sn(Oct)_2$) was used as catalyst in this process. Obtained PPF-*co*-PLLA copolymers were then dissolved in methylene chloride, precipitated in diethyl ether, and fully dried under vacuum. Molecular weights of PPF and PPF-*co*-PLLA copolymers were determined using gel permeation chromatography (GPC) carried out by a Viscotek GPCMax/VE 2001 GPC (Malvern Instruments, Inc.) connected to a model 2410 refractive index detector. Tetrahydrofuran (THF) was used as eluent at a flow rate of 1 mL min^{-1} and universal calibration system were applied in the calculation of molecular weight. The chemical structures of synthesis products were confirmed by ^{1}H NMR spectra recorded in a 300 MHz Varian NMR in $CDCl_3$ solvent.

Determination of cloud point and gelation curve

The microporous PPF-*co*-PLLA scaffolds were fabricated by liquid–liquid phase separation method from a PPF-*co*-PLLA/dioxane/water system. The cloud points for the ternary system were determined by visual turbidimetry, as described previously.[25] In brief, certain amount of PPF-*co*-PLLA copolymers (1, 3, 5, 7 and 9%) was fully dissolved by heating at 70 °C for 2 h in the dioxane/water binary solvents with different wt/wt ratios (85/15, 87/13, or 90/10). These clear solutions were slowly cooled at a rate of 1 °C per 10 min. The cloud-point temperature was determined as the temperature at which the clear solutions started to become turbid. Gelation temperatures were determined as the temperatures when solutions ceased to flow even though the vials were inverted horizontally, as described previously.[26,27]

Fabrication and characterization of 3-D porous scaffolds

Weighted PPF-*co*-PLLA (3, 5, or 9 wt%) were mixed with 1,4-dioxane/water (83/17, 85/15, or 87/13, wt/wt) binary system in 4-ml vials. The ternary PPF-*co*-PLLA /dioxane/water systems were heated to 65 °C for 20 min for polymers to dissolve, followed by 10 min incubation at a temperature 15 °C above the cloud point. Vials with dissolved PPF-*co*-PLLA were then quickly dipped into a quenching water bath at 20 °C. Quenching time was varied for 1, 4 and 8 min to determine the coarsening effect. The quenched samples were transferred to a freezing environment with temperatures of −20, −80 or −196 °C. Final 3-D porous scaffolds were extracted after removing solvents by lyophilization for 3 days. The morphology of the scaffolds was characterized using scanning electron microscopy (SEM; S-4700, Hitachi Instruments, Tokyo, Japan) at a voltage of 3.0 kV. To observe the internal structures of microporous scaffold, the samples were frozen in liquid nitrogen for 10 min and then broken open using forceps. Thermal properties of the PPF-*co*-PLLA scaffolds with different quench times were characterized using Differential Scanning Calorimetry (DSC, TA Instruments) measurements, in which the samples were heated from to 0 to 200 °C at a rate of 10 ºC/min.

The porosity of the scaffolds was determined according to previous reports.[28-30] Briefly, dried PPF-*co*-PLLA scaffolds fabricated with varied polymer concentration were weighed to obtain sample mass, marked as W_s. A pycnometer filled full of ethanol was weighed together as W_1. After immersion of porous polymer samples, the ethanol liquid started to invade the porous spaces originally occupied by air. Pycnometer was then filled full and its weight together with the polymer samples was marked as W_2. Then polymer scaffolds were taken out and the pycnometer was weighed again with the remaining ethanol to obtain W_3. The porosity was calculated according to the following equations:

$$V_t = \frac{(W_1 - W_3)}{\rho} \tag{1}$$

$$V_p = \frac{(W_2 - W_3 - W_s)}{\rho} \tag{2}$$

$$P = \frac{V_p}{V_t} = \frac{(W_2 - W_3 - W_s)}{(W_1 - W_3)} \tag{3}$$

where V_t is total volume, V_p is pore volume, P is porosity, and ρ is density of ethanol (0.789 g/mL).

Mechanics, degradation and protein adsorption

Mechanical properties of polymer scaffolds were analyzed from compressive strain-stress curves determined on a dynamic mechanical analyzer (DMA2980, TA instruments). PPF-*co*-PLLA scaffolds (5 × 5 mm, thickness × diameter) were compressed at a rate of 1.0 newton (N) per min up to an ultimate compressive force of 18 N. Compressive moduli were calculated from the stress–strain curves converted from the force-displacement values and averaged for five samples in each group. For degradation study, PPF-*co*-PLLA scaffolds were immersed in 0.1 M NaOH solution. The mass of PPF-*co*-PLLA scaffolds were measured every two days. To analyze the

ability of interconnected porous PPF-*co*-PLLA scaffolds to adsorb serum proteins, a series of porous scaffolds were immersed in Dulbecco's modified eagle medium (DMEM) with 10% fetal bovine serum (FBS) at 37 °C. Solid PPF-*co*-PLLA substrates were used as control group in this process. Then the samples were taken out, washed with 1 × phosphate buffered saline (PBS) for three times to remove the surface residue proteins, followed by three times wash with 200 μL 1% sodium dodecyl sulfate (SDS, Bio-Rad Laboratories, Inc.) to collect the adsorbed proteins. A micro-plate reader (SpectraMax Plus 384, Molecular Devices, Sunnyvale, CA) with MicroBCA protein assay kit (Pierce, Rockford, IL) were used in detecting the optical density (OD) values of these solutions.[31] The final protein amount correlated with OD were calculated using a standard curve generated by known concentrations albumin solutions.

Results and discussion

Polymers, cloud points and gelation curves

Poly(propylene fumarate) was synthesized from biologically compatible diethyl fumarate and 1,2-propylene glycol. The number average molecular weight (M_n), weight average molecular weight (M_w) and polydispersity index (*PDI*) for the obtained PPF product were determined to be 2260, 5240 and 2.3, respectively. PPF-*co*-PLLA triblock copolymers synthesized from ring opening reaction of caprolactone monomers using PPF as initiator were determined to have a yield of 95%. Purified PPF-*co*-PLLA was calibrated by GPC to have M_n, M_w and *PDI* values of 49050, 115200 and 2.3, respectively.
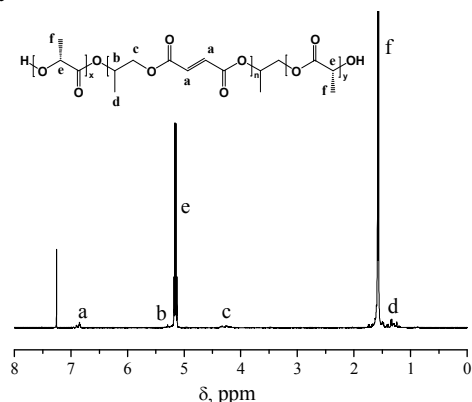
Fig. 2 ^{1}H NMR spectrum of PPF-*co*-PLLA triblock copolymer.

The chemical structure of PPF-*co*-PLLA triblock copolymer was detected using ^{1}H NMR spectra. As marked in polymer structure from Fig. 2, all chemical shifts in the ^{1}H NMR spectra could be well assigned to corresponding protons, indicating a precise structure for synthesized PPF-*co*-PLLA triblock copolymer.
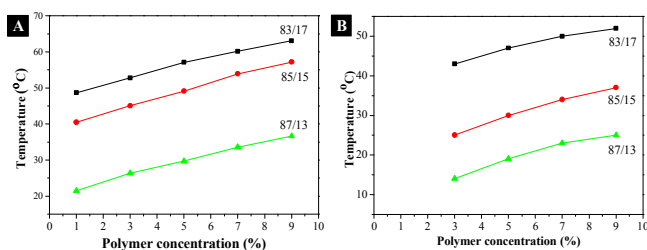
Fig. 3 (A) The cloud point, (B) gelation temperature determined for PPF-*co*-PLLA at varied polymer concentrations (1, 3, 5, 7 and 9

wt%) in a dioxane/water binary solvent (83/17, 85/15, and 87/13 wt/wt).

The dependence of solution cloud points and gelation temperatures on the PPF-*co*-PLLA concentrations, and the mass ratios of dioxane and water in the solvents were studied. As demonstrated in Fig. 3A, cloud points of the solutions increased with the increase of the PPF-*co*-PLLA concentration from 1 to 3, 5, 7, and 9 % in the solution. On the contrary, the increase of dioxane content in the dioxane/water binary system caused a decrease in the cloud points. Similar trend was observed for the gelation temperatures determined for these ternary PPF-*co*-PLLA/dioxane/water systems. However, in the solutions with 1% PPF-*co*-PLLA polymer, no detectable gelation was determined due to low concentration of polymer contents.

Effect of phase separation parameters

The influences of polymer concentration on the morphology, porosity, and compressive modulus of the PPF-*co*-PLLA scaffolds were studied. As demonstrated in Fig. 4, characteristic porous structures were observed for all systems after quenching. However, the interconnectivity of pore structures in scaffold decreased continuously with the increase of polymer concentrations from 3 to 5 and 9%, as shown in Fig. 4A, B, and C, respectively. A similar decreasing trend was determined for porosities of scaffolds fabricated with varied polymer concentrations. For scaffolds prepared by 3, 5, 7 and 9% of PPF-*co*-PLLA polymers, the porosities in the scaffolds were calculated to decreasing from 91.44 ± 1.34%, to 86.75 ± 1.16%, 83.58 ± 0.62%, and 81.16 ± 0.89%, respectively.
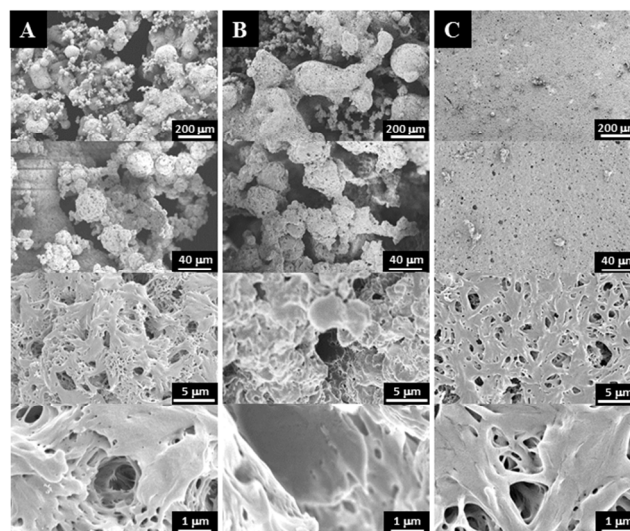
Fig. 4 SEM micrographs of 3-D porous scaffolds prepared by phase separation using: (A) 3 wt%, (B) 5 wt%, and (C) 9 wt% of PPF-*co*-PLLA in a dioxane/water (85/15 wt/wt) solution followed by quenching at 20 °C for 1 min, freezing at −80 °C for 2 hours and lyophilization for 3 days.

The gelation process of the polymer/dioxane/water ternary system is critical for obtaining unique nanofibrous structures. Fig. 5 demonstrates the morphological variance of the PPF-*co*-PLLA scaffolds prepared by heating the ternary PPF-*co*-PLLA /dioxane/water system to a temperature 15 °C above the could point then quenching in a 20 °C water bath for 1, 4, or 8 min. As seen from Fig. 5A, when the ternary PPF-*co*-PLLA /dioxane/water system was quenched for a short time of 1 min, open microporous structures were formed with solid pore walls. Higher magnification SEM

images demonstrated unique flower-shaped interconnected structures for these scaffolds from the submicron level. This unique structure is largely believed to be a characteristic of early stage phase separation, which is undergoing spinodal decomposition process[32]. With the increase of quenching time to 4 min, better interconnectivities inside the scaffolds were observed from SEM images in micron level for these PPF-*co*-PLLA scaffolds (Fig. 5B). When the quenching time increased to 8 min, PPF-*co*-PLLA scaffolds were observed to form specifically connected spherulite-like microspheres inside the matrix (Fig. 5C). An enlarged view of the microsphere surfaces revealed a more smooth topography without forming the flower-shaped morphologies, as compared to scaffolds with a shorter quenching time shown in Fig. 5A. These morphologies are formed predominately due to the coarsening process in the ternary system during the long quenching time. Further, the walls of formed microspheres are unique nanofibrous shape instead of being solidified.
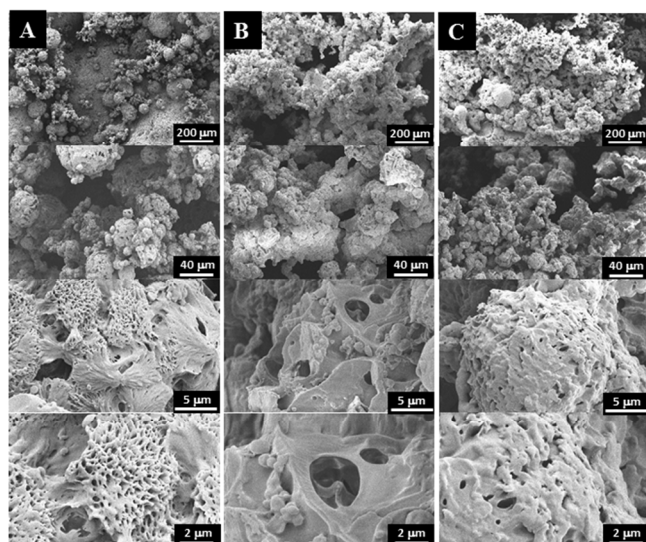
Fig. 5 SEM micrographs of 3-D porous scaffolds prepared by phase separation of 5% PPF-*co*-PLLA in dioxane/water (85/15 wt/wt) solution as a function of quench time: (A) 1 min, (B) 4 min, and (C) 8 min at 20 °C. The quenched samples were then frozen at −80 °C for 2 hours and dried by lyophilization for 3 days.
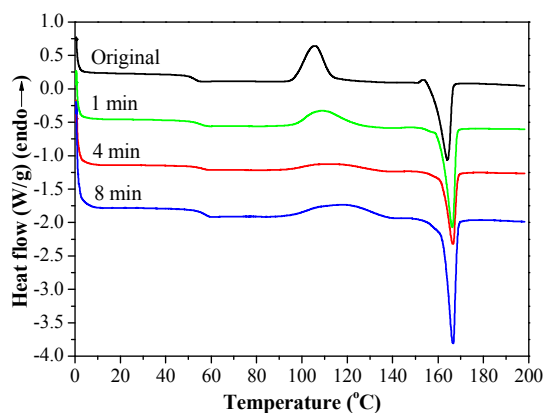
Fig. 6 DSC curves of PPF-*co*-PLLA in dioxane/water (85/15 wt/wt) solution quenched for 1, 4 and 8 min at 20 °C, with comparison to the original PPF-*co*-PLLA samples without quenching.

The thermal properties of the original PPF-*co*-PLLA and the PPF-*co*-PLLA scaffolds after 1, 4, and 8 min of quench time at 20 °C

were demonstrated in Fig. 6. As seen from the DSC curves obtained by the heating run from 0 to 200 °C, all the samples experienced glass transition, crystallization and melting processes. Their thermal properties including melting temperature (T_m), enthalpy (ΔH_m), and degree of crystallinity (χ_c) were calculated from these DSC curves and listed in Table 1. After quenching, the glass transition temperature of PPF-*co*-PLLA samples (1, 4 and 8 min) increased as compared to the original PPF-*co*-PLLA polymers (Table 1). T_m was the highest peak temperature in all the exothermal peaks. As shown in Fig. 6, the melting peaks of these scaffolds were found to shift from 164 °C to approximately 166 °C after quenching. It is largely believed that these melting peaks are the consequences of PPF-*co*-PLLA polymer chain crystallization in dioxane/water binary solution. The enthalpy (ΔH_m) for these melting peaks as well as crystallization peaks at lower temperatures were calculated from the DSC curves. Crystallinity (χ_c) was estimated using the following equation:

$$\chi_c = \frac{\Delta H_m}{\Delta H_0} \times \varphi_{PLLA} \times 100\%$$

where ΔH_0 was the enthalpy for fully crystalline PLLA with a value estimated as 93.6 J/g,[33] and φ_{PLLA} was the PLLA fraction in the copolymer, which was approximately 0.95. As noted from Table 1, the degree of crystallinities for polymer chains in the original PPF-*co*-PLLA was 3.8%. However, after an annealing process of 1, 4 and 8 min, the chain crystallinities increased to 17.5, 29.0 and 18.5%, respectively. This partial crystallization in polymer chains is believed to contribute to the increase of solution viscosity and induction of gelation in the ternary PPF-*co*-PLLA /dioxane/water system.

Table 1 Thermal properties of PPF-*co*-PLLA scaffolds annealed in dioxane/water system for different time.

Anneal time	T_g (°C)	T_m (°C)	$T_{Crystallizing}$ (°C)	$\Delta H_{Crystallizing}$ (J/g)	$\Delta H_{Melting}$ (J/g)	χ_c (%)
Original	52.6	164.0	107.0	35.0	38.5	3.8
1 min	55.3	166.6	110.4	14.6	30.6	17.5
4 min	56.4	166.6	118.3	24.9	51.5	29.0
8 min	54.3	166.2	108.9	25.5	42.4	18.5
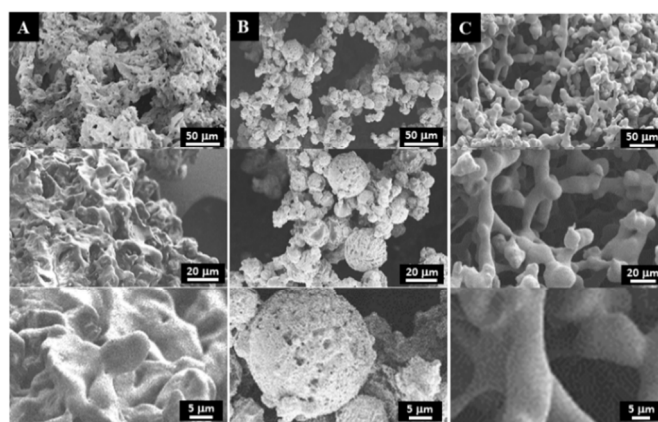
Fig. 7 SEM micrographs of 3-D porous scaffolds prepared by phase separation of 7% PPF-*co*-PLLA in dioxane/water (85/15, wt/wt) solution with freezing temperature of (A) −20 °C, (B) −80 °C, and (C) −196 °C.

To study the effect of freezing temperature on the morphologies of 3-D scaffolds, the 7% PPF-*co*-PLLA in dioxane/water (85/15, wt/wt) solution was frozen at different temperature of −20 °C, −80 °C (freezer) or −196 °C (liquid nitrogen). Pore morphologies created under these temperatures were observed by SEM and shown in Fig.

7. Compared to scaffolds fabricated from highest freezing temperature of −20 °C (Fig. 7A), scaffolds under low freezing temperatures of −80 and −196 °C appeared to gain better interior interconnectivities (Fig. 7B,C). It is also noticeable from micron level images that the scaffolds frozen in high temperatures have surfaces that largely melted during the drying process. It is imaginable that scaffolds frozen at −20 °C are easy to melt during the lyophilization process thus it is easy to diminish surface patterns. By decreasing the temperature to −80 °C or −196 °C in liquid nitrogen, the dioxane/water solution was frozen immediately, preserving the original distribution profile of PPF-*co*-PLLA chains in the solution. However, scaffolds frozen at −80 °C showed ball-shaped sphere structures while elongated rod-shaped structures with a relative smooth surface were created in scaffolds frozen at −196 °C. This phenomenon is largely owing to the movement of polymer chains, e.g., rotations, contractions, and sedimentations, continued for a longer time in the ternary PPF-*co*-PLLA/dioxane/water solution placed in freezer (−80 °C) rather than that in liquid nitrogen (−196 °C).
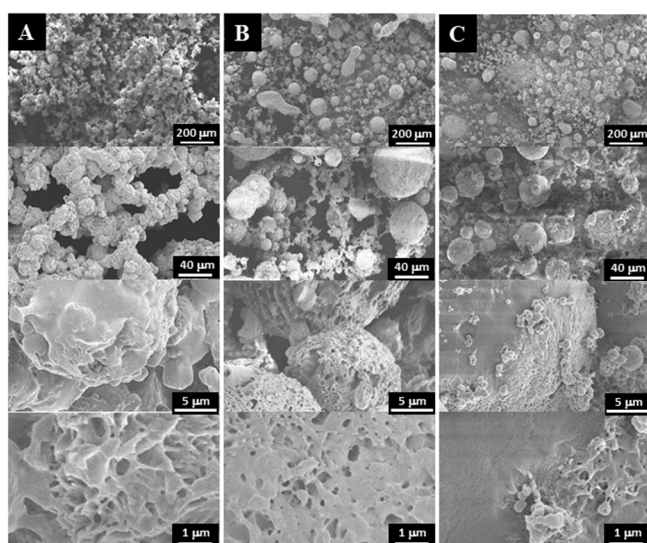
Fig. 8 SEM micrographs of 3-D porous scaffolds prepared by phase separation of 5% PPF-*co*-PLLA in a dioxane/water solution with varied weight compositions of (A) 83/17, (B) 85/15, and (C) 87/13. These samples were quenched at 20 °C for 1 min, followed by frozen at −80 °C for 2 hours and lyophilization for 3 days.

The effect of dioxane/water solvent composition on scaffold morphology was determined and displayed in Fig. 8. For the system with higher water content (83/17 dioxane/water), PPF-*co*-PLLA scaffolds showed more extensive interconnectivities (Fig. 8A). At micrometer level, the PPF-*co*-PLLA polymer chains were observed to form small spheres for system with 83/17 (dioxane/water) composition. This phenomenon is primarily resulted from the decrease in polymer solubility due to the higher water content in the system. In comparison, systems with lower water content (85/15 and 87/13 dioxane/water) showed obvious phase separating profiles, including large elongated droplet shaped spheres and round bead-like spheres in the scaffold, as presented in Fig. 8B,C, respectively This is largely because the low water content in the system increased polymer solubility and inhibited the polymer/solvent de-mixing process. This allows longer time for polymer chains to precipitate from the solution while quick freeze treatment solidified the whole system thus captured the undergoing phase separation morphology. Enlarged view using SEM demonstrated larger value in size for these

spheres compared with those formed in system with higher water content (83/17 dioxane/water). Besides morphology variances, decreases in water content in the PPF-*co*-PLLA /dioxane/water ternary systems also resulted in a lower cloud-point temperature, as displayed in Fig. 3A. The reasons for these phenomena are closely related to the solubility of PPF-*co*-PLLA in the system. Less solubility makes it easier for the polymer chains to form coils and precipitate from the solution. On the contrary, higher solubility prevents polymer chains to precipitate thus increasing the cloud point and gelation points. In addition, higher solubility increases the solution viscosity, which further decelerates the rate of phase separation in the thermally induced phase separation process.

Interconnected 3-D porous scaffolds properties

A series of 3-D tissue scaffolds were successfully fabricated by optimizing the processing conditions. Various shapes of scaffolds, including cylinders, tubes, discs, cubes and balls, were fabricated using different predesigned molds via the phase separation process, as presented in Fig. 9A. The surface morphology as well as internal pattern was determined using SEM. As presented in Fig. 9B, the fabricated scaffold showed interconnected microporous network throughout the surface area and the internal space. At the submicron level, flower-shaped patterns were observed throughout the scaffold. Compared with the smooth surfaces achieved by conventional 3-D printing or salt-leaching method, these porous structures can achieve higher total surface area. In previous reports, the high surface area of tissue scaffolds was determined to increase protein adsorption thus further promote cellular attachment.[34]
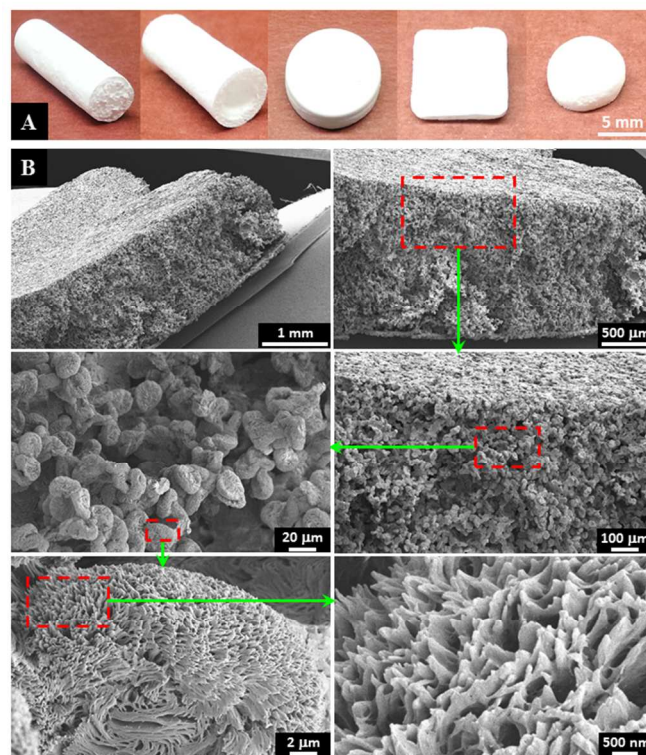
Fig. 9 (A) Different shapes of 3-D PPF-*co*-PLLA scaffolds fabricated by phase separation of 9% PPF-*co*-PLLA in dioxane/water (83/17 wt/wt) binary system, annealed for 1 min, and frozen at −80 °C for 2 hours, (B) interconnected porous structures determined using SEM at micron and submicron level.

The compressive mechanical properties of the fabricated PPF-*co*-

PLLA scaffolds were determined after favorable morphologies were observed for tissue engineering applications. Solid PPF-*co*-PLLA scaffolds were used as controls in this process. As can be seen from the stress-strain curves in Fig. 10A, PPF-*co*-PLLA samples were deformed under an ultimate compressive force of 18 N. However, the extent of deformation varied. For interconnected PPF-*co*-PLLA scaffold, a typical compressive stress-strain curve for porous samples was detected (Fig. 10A). This curve is composed of a linear region, a flat region, and a densified region.[35,36] The linear elastic region (0 to 10% strain) represents the linear elastic deformation of the porous PPF-*co*-PLLA samples. The flat region (10 to 35% strain) was the plateau region of deformation at larger strain. The final densified region (> 35% strain) occurred under strong compression. At this stage, the scaffold was increasingly solidified due to the collapse of pore walls, resulting in a sharp increase in the compressive stress. The compressive modulus determined from the stress-strain curves for PPF-*co*-PLLA scaffolds was 3.39 ± 0.46 MPa. For the solid PPF-*co*-PLLA without porous structures, only a linear region was observed in the stress-strain curve. The compressive modulus was determined to have value of 21.38 ± 3.46 MPa. These PPF-*co*-PLLA scaffolds possessed sufficient mechanical support (3.4 to 21.4 MPa) for the repair and regeneration of damaged or diseased trabecular bones, which has a compressive modulus in a region of 2-20 MPa.[37,38]
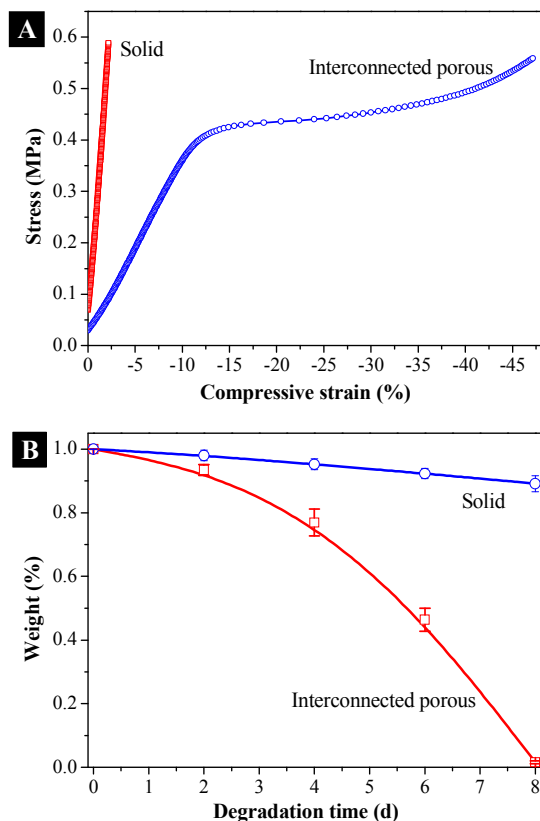
Fig. 10 (A) Compressive stress-strain curves determined for solid and porous 3-D porous PPF-*co*-PLLA scaffolds, (B) degradation curves for solid and porous 3-D porous PPF-*co*-PLLA scaffolds in 0.1 M NaOH solution.

Biodegradability is another crucial factor for polymeric scaffolds aiming at bone regeneration in tissue engineering applications.[39] Ideal scaffolds are expected to have not only appropriate mechanical strengths but also capabilities to degrade *in vivo* at certain rate thus leaving space for the newly generated bone tissue to grow into.

Based on different applications, the need for scaffold degradation time varies, preferably 3-9 months, more or less, for scaffolds prepared for bone tissue regeneration.[40] However, the reported degradation time for PLLA is normally larger than 24 months.[41] Clinical studies even found that high crystalline PLLAs remained within patients body at 5.7 years after implantation.[42] The accelerated degradation test in our study demonstrated a degrading period of 8 days for interconnected porous PPF-*co*-PLLA scaffolds in 0.1 M NaOH solution. For solid substrate control however, only a slight surface erosion but no obvious bulk degradation was determined within the same time scale, as displayed in Fig. 10B. The interconnected porous structures therefore improved the solution transportations into the interior of scaffolds and facilitated the bulk degradation of polymeric scaffolds in solution. Degradation in phosphate-buffered saline (PBS) and *in vivo* conditions is currently under way.
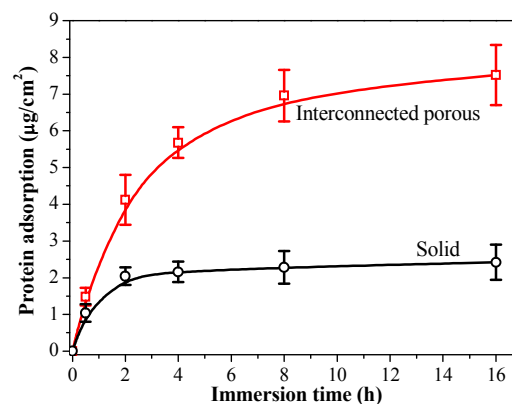
Fig. 11 Serum protein adsorption on solid and 3-D porous PPF-*co*-PLLA scaffolds in DMEM cell culture medium added with 10% FBS.

Proteins play crucial roles in mediating cellular recognition and adhesion to synthetic matrixes.[43] For polymeric scaffolds without cellular binding ligands incorporated onto the surface, they require the adsorption of external proteins from cell culture medium for cell attachment. After implantation, the tissue scaffold will be exposed to body fluids that may contain various serum proteins. Thus, the ability of a scaffold to adsorb serum protein is pivotal in evaluating its biocompatibility and bioactivity. As demonstrated in Fig. 11, the amounts of proteins adsorbed within 2 hours in the interconnected porous PPF-*co*-PLLA scaffolds were significantly higher than that on solid substrates with flat surface. This phenomenon is believed to be caused by the larger contract area for porous PPF-*co*-PLLA scaffolds with the serum proteins in the culture media, which promotes protein adsorption. After 2 hours, no further protein adsorption was observed on the solid substrates. However, for the interconnected porous PPF-*co*-PLLA scaffolds, continuous protein adsorptions at a slower rate from cell culture media were detected (Fig. 11). This is largely due to the infiltration of medium into the interconnected porous structures, which induced the sediment of serum proteins inside the scaffold. These scaffolds fabricated using optimum phase separation parameters thus improve the medium transport capabilities and protein adsorption abilities, and may be potentially useful for tissue engineering applications by absorbing larger amount of proteins and growth factors.[44] Further experiments will be carried out to determine the ability of the porous scaffold to support cell attachment, proliferation, and differentiation *in vitro*.

In summary, biodegradable PPF-*co*-PLLA triblock copolymer was synthesized and successfully fabricated into 3-D porous scaffolds through phase separation process. Compared to the limited reports

using pure PCL or PLLA polymers,[25,27,29] our study extends the TIPS fabrication of tissue scaffolds from singular polymer to boarder copolymers. In addition, the effects of various processing parameters on scaffold fabrication were investigated and the optimized processing condition was determined, which will be useful for future reproduction and *in vitro* or *in vivo* applications of 3-D porous copolymer scaffolds. The interconnected porous structures inside the scaffold were also characterized. The collapse of thin pore wall layers under compressive stress was found to strengthen the elastic properties of the scaffold. The enhanced elasticity and attenuated stiffness of the PPF-*co*-PLLA 3-D porous scaffold may render useful as a supporting matrix for soft tissue regenerations. Furthermore, the interconnected porous structures facilitate the infiltration of media into the interior part of the scaffold, which substantially increases the contact area between scaffold and medium and consequently leads to higher protein adsorption and faster degradation for the scaffold. Compared with inorganic or carbohydrate materials,[45] the newly developed PPF-*co*-PLLA polymer reported in this study has the advantages of facile synthesis, desirable mechanical properties and faster degradation by hydrolysis of the ester group in polymer backbone. Therefore, this work provides a facile route for various polymers and copolymers to fabricate multi-dimensional porous scaffolds for tissue engineering applications.

Conclusions

Biodegradable PPF-*co*-PLLA scaffolds with highly interconnected porous structures were fabricated from a ternary polymer/dioxane/water system by thermally induced spinodal liquid–liquid phase separation. The influence of formulation and processing parameters including polymer concentration, quench time, solvents composition, and freeze temperature on scaffold morphology were studied thoroughly. The results showed that the cloud point and gelation temperature of ternary PPF-*co*-PLLA/dioxane/water system were significantly influenced by the polymer concentration and the ratio of 1,4-dioxane to water. Further adjusting the phase separation conditions resulted in remarkable differences in subsequently formed porous scaffolds in terms of porosity, morphology, thermal, and mechanical properties. The optimum processing parameters obtained were then successfully applied to fabricate a series of porous scaffolds in different shapes, which demonstrated mechanic strength, degradation rates and protein adsorption capabilities that are highly demanded in tissue engineering applications. The optimized phase separation method reported in this study may be applied to other polymers and copolymers to fabricate multi-component and multi-dimensional tissue scaffolds.

Acknowledgements

Notes

aDepartment of Orthopedic Surgery, Mayo Clinic, Rochester, MN 55905, USA. Email: Lu.Lichun@mayo.edu

bDepartment of Physiology and Biomedical Engineering, Mayo Clinic, Rochester, MN 55905, USA

References

1   R. Langer and J. P. Vacanti, *Science*, 1993, **260**, 920.

2   P. X. Ma, *Adv. Drug Deliver. Rev.*, 2008, **60**, 184.

3   P. M. Kharkar, K. L. Kiick and A. M. Kloxin, *Chem. Soc. Rev.*, 2013, **42**, 7335.

4   X. Liu and S. Wang, in *Encyclopedia of Biomedical Polymers and Polymeric Biomaterials*, ed. M. Mishra, Taylor & Francis, New York, USA, 2014, DOI:10.1081/E-EBPP-120051253

5   J. Z. Paxton, K. Donnelly, R. P. Keatch and K. Baar, *Tissue Eng. Part A*, 2009, **15**, 1201.

6   J. Nicolas, S. Mura, D. Brambilla, N. Mackiewicz and P. Couvreur, *Chem. Soc. Rev.*, 2013, **42**, 1147.

7   R. A. Thibault, L. Scott Baggett, A. G. Mikos and F. K. Kasper, *Tissue Eng. Part A.*, 2010, **16**, 431.

8   (a) M. T. Arafat, C. X. F. Lam, A. K. Ekaputra, S. Y. Wong, C. He, D. W. Hutmacher, X. Li and I. Gibson, *Soft Matter*, 2011, **7**, 8013. (b) L. Cai, C. J. Foster, X. Liu and S. Wang, *Polymer*, 2014, **55**, 3836.

9   (a) A. Guiseppi-Elie, C. Dong and C. Z. Dinue, *J. Mater. Chem.*, 2012, **22**, 19529. (b) C. N. Kotanen, A. N. Wilson, C. Dong, C. Z. Dinu, G. A. Justin and A. Guiseppi-Elie, *Biomaterials*, 2013, **34**, 6318.

10   Z. C. Xing, S. J. Han, Y. S. Shin, T. H. Koo, S. Moon, Y. Jeong and I. K. Kang, *J. Biomater. Sci. Polym. Ed.*, 2013, **24**, 61.

11   I. Armentano, M. Dottori, E. Fortunati , S. Mattioli and J. M. Kenny, *Polym. Degrad. Stabil.*, 2010, **95**, 2126.

12   J. P. Fisher, T. A. Holland, D. Dean, P. S. Engel and A. G. Mikos, *J. Biomater. Sci. Polym. Ed.*, 2001, **12**, 673.

13   S. Wang, L. Lu and M. J. Yaszemski, *Biomacromolecules*, 2006, **7**, 1976.

14   (a) J. Yan, J. Li, M. B. Runge, M. Dadsetan, Q. Chen, L. Lu and M. J. Yaszemski, *J. Biomater. Sci. Polym. Ed.*, 2011, **22**, 489. (b) X. Gong, *Phys. Chem. Chem. Phys.*, 2013, **15**, 10459. (c) X. Gong, *RSC Adv.*, 2014, **4**, 54494

15   B. Dhandayuthapani, Y. Yoshida, T. Maekawa and D. S. Kumar, *Int. J. Polym. Sci.*, 2011, **2011**, 1.

16   H. Tamai, K. Igaki, E. Kyo, K. Kosuga, A. Kawashima, S. Matsui, H. Komori, T. Tsuji, S. Motohara and H. Uehata, *Circulation*, 2000, **102**, 399.

17   R. Waksman, *J. Interv. Cardiol.*, 2006, **19**, 414.

18   S. He, M. D. Timmer, M. J. Yaszemski, A. W. Yasko, P. S. Engel and A. G. Mikos, *Polymer*, 2001, **42**, 1251.

19   L. Cai and S. Wang, *Biomaterials*, 2010, **31**, 7423.

20   K. Wang, L. Cai, F. Hao, X. Xu, M. Cui and S. Wang, *Biomacromolecules*, 2010, **11**, 2748.

21   G. Mikos and J. S. Temenoff, *Electron. J. Biotechnol*, 2000, **3**, 114.

22   J. M. Holzwarth and P. X. Ma, *Biomaterials*, 2011, **32**, 9622.

23   S. A. Martel-Estrada, C. A. Martinez-Perez, J. G. Chacon-Nava, P. E. Garcia-Casillas and I. Olivas-Armendariz, *Mater. Lett.*, 2011, **65**, 137.

24   S. Wang, D. H. Kempen, M. J. Yaszemski and L. Lu, *Biomaterials*, 2009, **30**, 3359.

25   L. Budyanto, Y. Q. Goh and C. P. Ooi, *J. Mater. Sci. Mater. Med.*, 2009, **20**, 105.

26   B. M. Jeong, D. S. Lee, J. I. Shon, Y. H. Bae and S. W. Kim, *J. Polym. Sci. A*, 1999, **37**, 751.

27   F. J. Hua, G. E. Kim, J. D. Lee, Y. K. Son and D. S. Lee, *J. Biomed. Mater. Res.*, 2002, **63**, 161.

28   H. She, X. Xiao and R. Liu, *J. Mater. Sci.*, 2007, **42**, 8113.

29 S. Liu, Z. He, G. Xu and X. Xiao, *Mater. Sci. Eng. C Mater. Biol. Appl.*, 2014, **44**, 201.

30 J. R. Oppenheimer, A. G. Martin and L. P. Walker, *Bioresource Technol.*, 1997, **59**, 241.

31 L. Cai and S. Wang, *Polymer*, 2010, **51**, 164.

32 P. V. D. Witte, P. J. Dijkstra, A. W. V. Ber and J. Feijen, *J. Membr. Sci.*, 1996, **117**, 1.

33 A. Celli and M. Scandola, *Polymer*, 1992, **33**, 2699.

34 K. M. Woo, V. J. Chen and P. X. Ma, *J. Biomed. Mater. Res. A*, 2003, **67**, 531.

35 Y. Wan, X. Cao, Q. Wu, S. Zhang and S. Wang, *Polym. Adv. Technol.*, 2008, **19**, 114.

36 L. Liu, Z. Xiong, Y. Yan, Y. Hu, R. Zhang and S. Wang, *J. Biomed. Mater. Res. A*, 2007, **82**, 618.

37 D. E. T. Shepherd and B. B. Seedhom. *Rheumatology*, 1999, 38, 124.

38 N. Rotter, M. Bücheler, A. Haisch, B. Wollenberg and S. Lang, *J. Tissue Eng. Regen. Med.*, 2007, **1**, 411.

39 D. F. Williams, *Biomaterials*, 2008, **29**, 2941.

40 S. Bose, M. Roy and A. Bandyopadhyay, *Trends Biotechnol.*, 2012, **30**, 546.

41 J. C. Middleton and A. J. Tipton, *Biomaterials,* 2000, **21**, 2335.

42 J. E. Bergsma, W. C. de Bruijn, F. R. Rozema, R. R. M. Bos and G. Boering, *Biomaterials*, 1995, **16**, 25.

43 R. Ayala, C. Zhang, D. Yang, Y. Hwang, A. Aung, S. S. Shroff, F. T. Arce, R. Lal, G. Arya and S. Varghese, *Biomaterials*, 2011, **32**, 3700.

44 V. Guarino, A. Gloria, M. G. Raucci and L. Ambrosio, *Polymers*, 2012, **4**, 1590.

45 (a) Z. Yu, R. M. Schmaltz, T. C. Bozeman, R. Paul, M. J. Rishel, K. S. Tsosie and S. M. Hecht, *J. Am. Chem. Soc.*, 2013, **135**, 2883. (b) Z. G. Estephan, Z. Qian, D. Lee, J. C. Crocker and S. J. Park, *Nano Lett.*, 2013, **13**, 4449. (c) B. R. Schroeder, M. I. Ghare, C. Bhattacharya, R. Paul, Z. Yu, P. A. Zaleski, T. C. Bozeman, M. J. Rishel and S. M. Hecht, *J. Am. Chem. Soc.*, 2014, **136**, 13641. (d) M. M. Madathil, C. Bhattacharya, Z. Yu, R. Paul, M. J. Rishel and S. M. Hecht, *Biochemistry*, 2014, **53**, 6800. (e) Q. Xu, Y. Liu, C. Liu, A. Tian, X. Shi, C. Dong, Y. Zhou and H. Zhou, *RSC Adv.*, 2015, **5**, 14458.

RSC Advances Accepted Manuscript